Dense Water Dynamics along the Strait of Sicily (Mediterranean Sea)

M. ASTRALDI, G. P. GASPARINI, AND L. GERVASIO

Istituto per lo Studio dell'Oceanografia Fisica, CNR, La Spezia, Italy

E. SALUSTI

INFN, Dipartimento di Fisica, Università "La Sapienza," Rome, Italy

(Manuscript received 2 January 2000, in final form 1 May 2001)

ABSTRACT

Hydrographic and current meter data, gathered in different periods in the Strait of Sicily and in the southern Tyrrhenian Sea, allow the outflow characteristics from the eastern toward the Western Mediterranean basin to be analyzed. The evolution through the strait of a deep vein of dense water coming from the Eastern Mediterranean is described, together with the dynamic interaction with overlying layers. These data are related to a slightly generalized version of recent density current models, such as those of Emms and those of Baringer and Price. Taking into account the dynamic influence of the overlying currents, and in particular their friction and mixing, this model explains the path of this deep flow and enables estimates of entrainment and bottom friction to be made. With these new data, a phenomenon of considerable interest, namely the dynamics of density currents crossing and outflowing from a strait, is examined and discussed.

1. Introduction

The Strait of Sicily (Fig. 1) connects the Eastern and the Western Mediterranean basins. It has a minimum width of about 150 km and a length of about 600 km. At its northern boundary lies the rather irregular Sicilian shelf, while eastward there is the Tunisian shelf and the Malta Bank. Two sill systems delimit the strait: on the western side, two passages, respectively ~430 (section IV) and ~365 m deep (section V), connect the strait with the Western Mediterranean basin; on the eastern side the deep connection with the Ionian Sea is south of Malta Bank, across a sill ~560 m deep. The central region, the real deep part of the strait, is 50–100 km wide and 700–900 m deep with some trenches even reaching 1800 m.

The water masses present in this region are characterized by an eastward surface flow of Modified Atlantic Water (MAW) in the upper ~200 m, below which a westward flow of Levantine Intermediate Water (LIW) crosses the strait before entering the Tyrrhenian Sea. Recently a vein with slightly different characteristics was observed to flow immediately over the sea bottom, following approximately the same route as LIW (Astraldi et al. 1996). This dense water, fresher and colder than LIW, is present in the Ionian Sea filling the transitional layer between LIW and Eastern Mediterranean Deep Water. It was referred (Sparnocchia et al. 1999) to it as transitional Eastern Mediterranean Deep Water (tEMDW) but in the following we call it EMDW. At the entrance to the strait, its mean hydrographic characteristics are $T = 13.53$°C, $S = 38.723$ psu, and $\sigma_\theta \sim 29.17$. At the western exit of the strait this vein was observed to descend from a depth of ~300 m over the sill to a depth of ~1800 m in the southern Tyrrhenian Sea, along the Sicilian slope. This sinking process is made possible (also) because EMDW ($\sigma_\theta \sim 29.10$) is denser than the Tyrrhenian LIW ($\sigma_\theta \sim 29.05$). The pathway and the water characteristics of this current, together with its evolution, mixing, and entrainment, will be described here on the basis of data measured during four hydrographic cruises from 1993 to 1998.

A density current model related to some hydrographic and current observations is discussed herein. We are in particular interested in two intriguing physical effects: first, the sharp deepening of EMDW and, second, its crossing the strait midline or, more precisely, the inversion of the interface slope. Indeed, along its travel from the eastern to the western basin the cold dense EMDW vein, on reaching the western sill, does not flow along the Sicilian shelf but over the opposite shelf break along the Tunisian coast at an unexpectedly shallow depth, less than ~300 m, beneath a more vigorous westward LIW current. Subsequently, farther downstream, west of the sill where LIW decreases in velocity, the deep vein reestablishes its geostrophic position along

Corresponding author address: Dr. Ettore Salusti, INFN-Dip. to di Fisica, Universita La Sapienza, Piazzale A. Moro 2, Rome 00185, Italy.
E-mail: ettore.salusti@roma1.infn.it

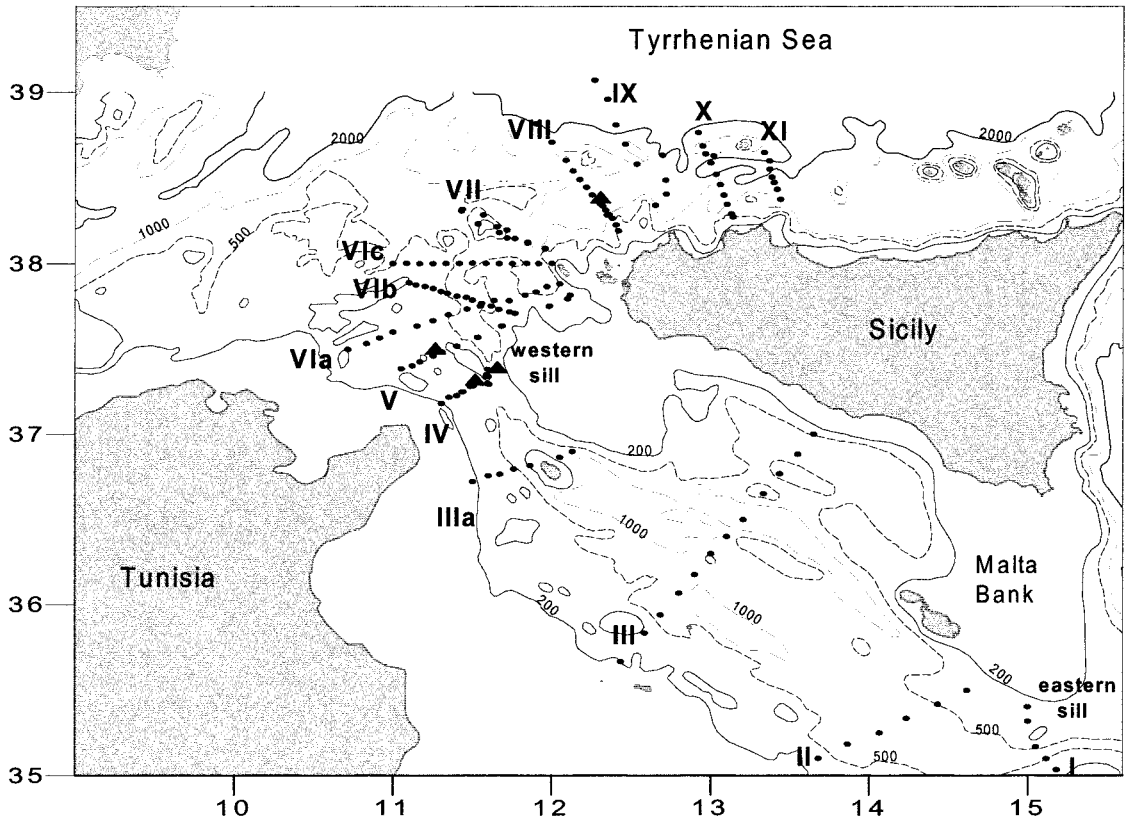

FIG. 1. Map of the Strait of Sicily. Dots represent the locations of the hydrographic stations (sections indicated by roman numerals); triangles indicate current meter positions.

the Sicilian coast but at a much deeper level (1500–1850 m deep).

This evolution of the interface slope is ultimately due to the geostrophic balance between buoyancy and Coriolis forces, depending on both the LIW and EMDW layer velocities. Note how the dynamic effect of the overlying flows, although not particularly novel, is an interesting mechanism for the deepening of the density currents that was not included in previous stream-tube models (Smith 1975; Killworth 1977; Bignami et al. 1990; Chapman and Gawrkiewicz 1995) and is somewhat reminiscent of classical analyses, such as that of Kinder and Bryden (1990) on Gibraltar.

So the vein dynamics are discussed here, paralleling a theoretical analysis of Emms (1997) and a careful inspection of deep baroclinic flows downstream from Gibraltar by Baringer and Price (1997a,b) in order to diagnose the properties and the processes influencing the flow of EMDW and, more specifically, the role played by entrainment and bottom stresses in modifying the vein characteristics. The role of the mixing of the upper layers in accelerating the bottom current, so as to allow the crossing of the channel sill, is examined on theoretical and experimental grounds, generalizing a recent model of Lane-Serff et al. (2000). Note also that in all these considerations internal modes and transient phenomena, as recently discussed by Pratt et al. (2000), have been disregarded.

2. The data

In the frame of different European Union Marine Science and Technology programme projects, different hydrographic measurements were obtained in the Strait of Sicily, Sardinia Channel, and the southern Tyrrhenian Sea to describe the various water mass characteristics. These measurements consisted of CTD profiles carried out using a Neil Brown MKIII CTD probe, calibrated before and after each cruise. The estimated precision was 5×10^{-3} for temperature and 2×10^{-3} for salinity. In addition, salinities of deep water samples were analyzed on board using a Guildline Autosal salinometer, and some direct current measurements were obtained on the western sills of the strait and at the southern entrance of the Tyrrhenian Sea (Fig. 1).

The in situ data cover different periods from November 1993 to May 1998: four hydrographic cruises will be considered here, together with current meter data.

a. PRIMO 93 cruise (Nov 1993)

The hydrographic measurements were made along sections that allow the progressive monitoring of the

TABLE 1. Main experimental quantities measured in the Strait of Sicily and in the southern Tyrrhenian Sea during the PRIMO 93 cruise. The geographical positions of the sections are shown in Fig. 2; we estimated $g' = g\Delta\rho/\rho$ as the difference in averaged layer densities (maximum plus minimum of ρ over two) of both EMWD and LIW; ρ_{bottom} is the maximum σ_θ observed in the hydrographic casts; dist is the distance between adjacent sections, and h is the bottom layer thickness. The other quantities are discussed in the text.

	Section				
	IV	V	VII	VIII	X
g' (m s^{-2})	8×10^{-4}	7×10^{-4}	6×10^{-4}	6×10^{-4}	6×10^{-4}
σ_{bottom}	29.150	29.145	29.125	29.123	29.120
h (m)	50	30	170	600	450
b (m)	400	280	1000	1700	1800
dist (km)	25	90	90	110	
W (km)	15	15	12	25	15
$\mathcal{A}_{EMDW}$ (km^2)	0.6	0.3	0.4	2.2	4.6
$\mathcal{A}_{LIW}$ (km^2)	7	14	18		

LIW and the EMDW outflows, starting from the western sill of the strait (Fig. 2). Current meter measurements are also available over the western sill (section IV) in correspondence with section VIII (Fig. 1). These data evidence for the first time the presence of a deep vein in the Eastern Mediterranean outflow. A detailed description of the hydrographic characteristics and a first discussion of the dynamics of the outflow can be found in Sparnocchia et al. (1999). The evolution of this bottom EMDW density clearly indicates how the vein moves through the strait along the Sicilian shelf break towards the Tyrrhenian Sea. At first (section IV) the vein is characterized by $\sigma_\theta \approx 29.15$ and, at its lowest depth (section V), reaches a density of ~29.14. Section IV has two passages, but the passage in section V is connected only with the westward passage. A subsequent decrease is found in section VII with $\sigma_\theta \approx 29.12$. The same σ_θ is also found in section X, when the vein leaves the bottom and reaches its buoyant equilibrium, lying at the level of resident Tyrrhenian Deep Water. The comparison among the different sections and, more specifically, between section V and X clearly shows the deepening of EMDW from ~300, over the sill, to ~1850 m depth in the southern Tyrrhenian Sea. It is important to observe that, in the vicinity of the sill, the vein is found only in the westward passage along the Tunisian slope (section IV), maintains this characteristic over the sill (section V), and inverts its slope only when it enters the Tyrrhenian Sea (section VII). The θ–S diagram (Fig. 2b) shows that the most substantial changes in the hydrographic characteristics are observed between the strait and the Tyrrhenian entrance, namely between sections V and VII.

Direct current measurements indicate that in section IV the EMDW current has an intensity of 12.5 ± 11.6 cm s^{-1}. Along section VIII the current is directed toward the Tyrrhenian Sea: the alongshore velocity is 17.9 ± 8.3 cm s^{-1} at about 500 m, 13.3 ± 6.5 cm s^{-1} at 900 m and 19.4 ± 10.3 cm s^{-1} at 1200 m. The two deepest velocities correspond to the LIW and EMDW veins, respectively. The cross-shore velocities are much smaller, and this supports a geostrophic description of these flows. The most important parameters describing the vein evolution, as well as quantifying the previous information on the hydrograhic characteristics more satisfactorily, indicate significant changes in the geometric dimensions of the vein, which are deeply influenced by the topography (Table 1). Its thickness, 50–100 m over the sill, increases to more than 500 m after the vein has reached its buoyant equilibrium (section X).

b. MATER 1 cruise (16 Sep–13 Oct 1996)

This dataset essentially covers the region between the strait and its Tyrrhenian entrance. The density values (Fig. 3a) do not display any significant changes with respect to the previous cruise. While the density in section IV is very similar to the PRIMO 93 cruise, in section V the interface slopes downward to the east. Section VI, not present in the previous cruise, shows a consid-

TABLE 2. As for Table 1 but relative to the MATER 1 cruise (Fig. 3).

	Section			
	IV	V	VIb	VII
g' (m s^{-2})	7×10^{-3}	7×10^{-3}	6×10^{-4}	5×10^{-4}
σ_{bottom}	29.153	29.148	29.121	29.123
h (m)	30	20	140	260
b (m)	530	300	750	1100
dist (km)	25	20	30	
W (km)	15	15	18	12
$\mathcal{A}_{EMDW}$ (km^2)	0.3	0.2	0.8	2.4
$\mathcal{A}_{LIW}$ (km^2)	7	16	15	18

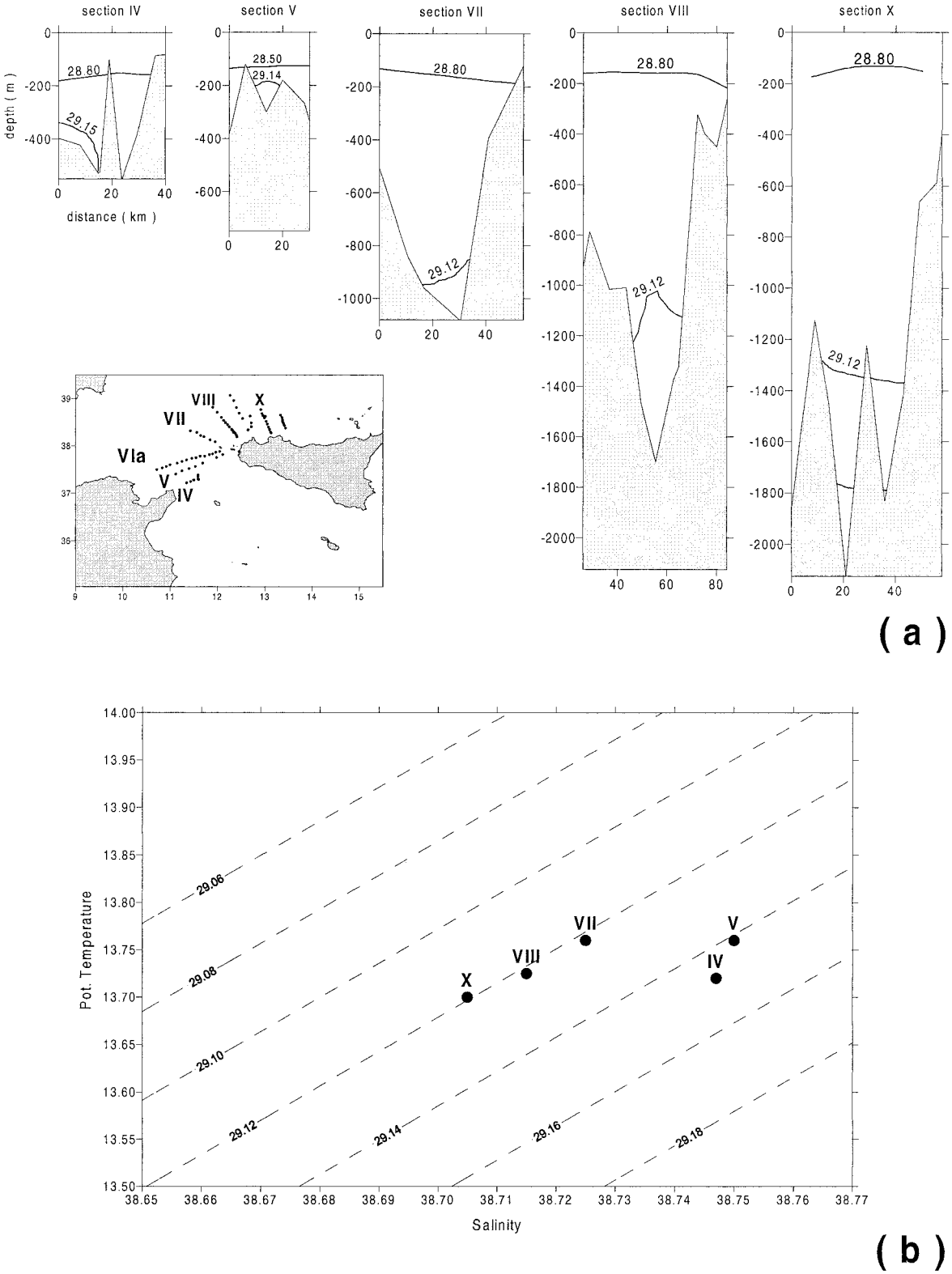

FIG. 2. PRIMO 93 cruise (Nov 1993) isopycnal cross-sections: (a) in each section interfaces between surface (MAW), intermediate (LIW), and deep (EMDW) layers are indicated. Note in addition that section IV has two passages, but only the western passage is connected with the EMDW passage of section V. The view of these sections is from the eastern toward the western basin: Sicily is always on the right-hand side. θ–S diagram (b) of EMDW hydrographic characteristics, close to the bottom.

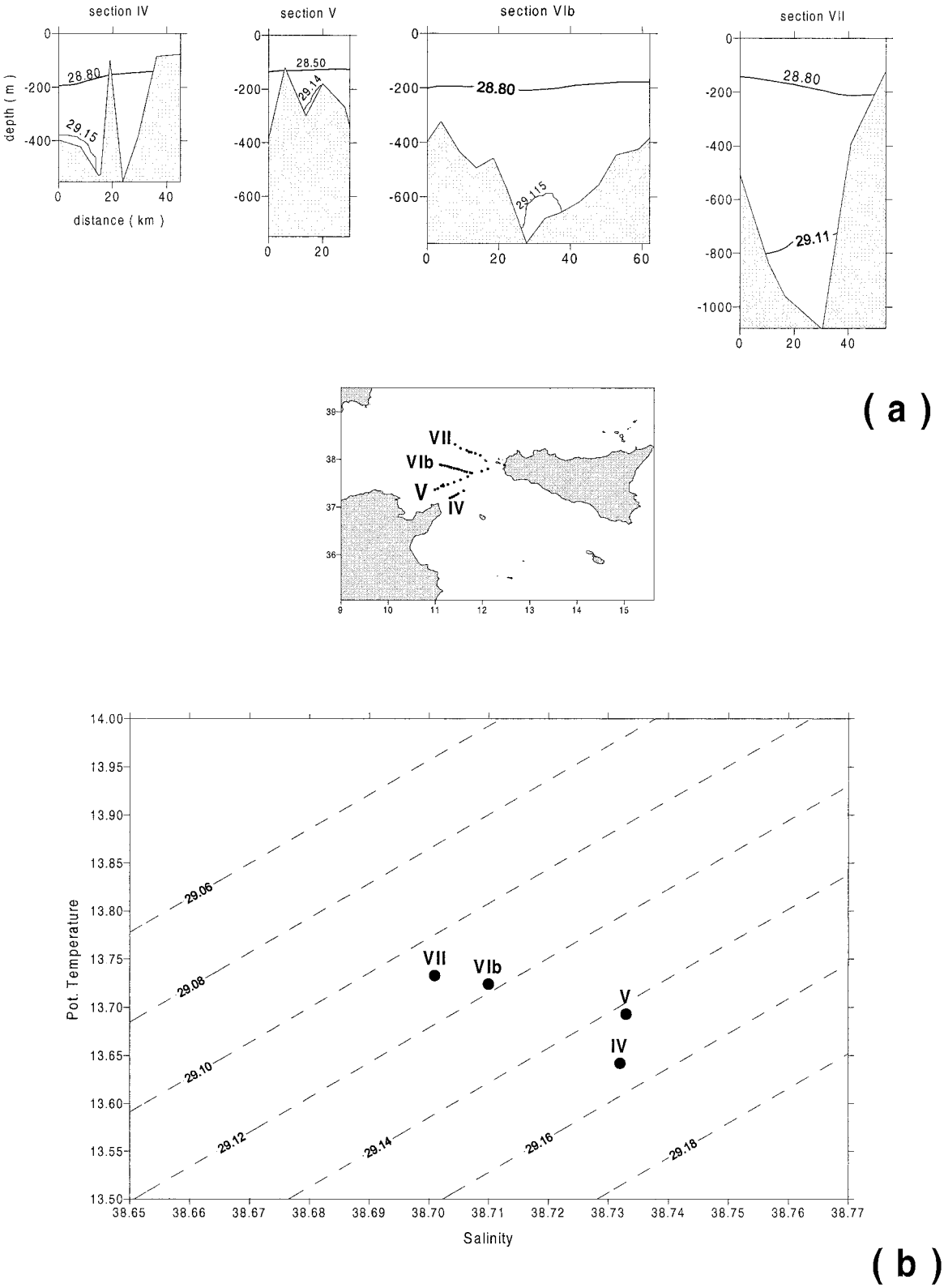

FIG. 3. As in Fig. 2 but for MATER 1 cruise (16 Sep–13 Oct 1996).

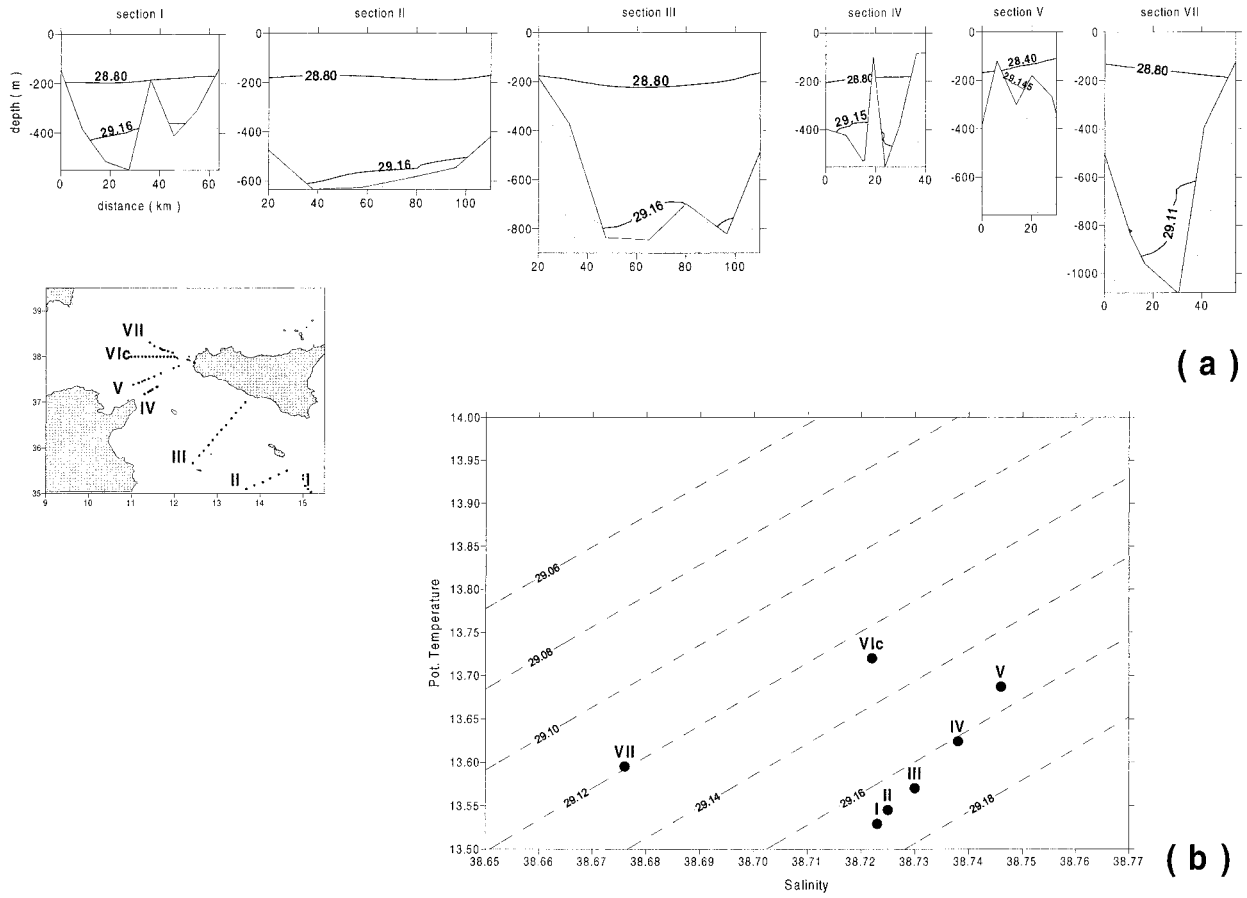

FIG. 4. As in Fig. 2 but for MATER 2 cruise (Jan 1997).

erable density decrease. This suggests that an important mixing region can be located immediately downstream from the sill. Between sections V and VI the largest sinking of the vein occurs, from ~370 m to ~750 m in depth, over a distance of only 25 km. The θ–S diagram (Fig. 3b) presents the same shape as observed on the previous cruise and confirms the isopycnal evolution (Fig. 3a). After the significant change at the western sill, between sections V and VIb, the hydrographic characteristics of the vein seem to be very close to buoyant equilibrium. Table 2 summarizes the principal properties of the vein and indicates that its geometry does not present any significant changes with respect to PRIMO 93. Conversely, a comparison among the hydrographic parameters indicates a significant decrease both in temperature and salinity, which corresponds to a weak overall increase in density.

c. MATER 2 cruise (Jan 1997)

These hydrographic stations cover the region from the eastern sill (Malta sill), the basin interior, and across the western sill (Sicily–Tunisia sill), as far as the southern Tyrrhenian Sea (Fig. 4). While the previous cruises evidenced the peculiar dynamics of the dense vein downstream of the western sill of the strait, this and the following cruise allow attention to be focused on the dynamics along the strait and especially around the western sills. The isopycnal signature of EMDW can be followed through the channel (Fig. 4a).

This EMDW enters the basin at the deepest passage of the Malta sill at a depth of 500–550 m along the Sicilian shelf (section I). Inside the basin, besides filling two deep trenches (Fig. 1), it flows along the African side of the strait at a depth of about 700–800 m (section III). Farther westward, the vein rises up to depth 500 m (section IV) and 350 m (section V) over the African shelf. Note that over this distance of ~320 km the vein presents only weak changes: σ_θ decreases from 29.16 to 29.145, while the isopycnal inclination gives a geostrophic westward flow. It is also worth noting that sections IV and V show an opposite isopycnal slope, which switches back into the usual position only over section VII. Along the same section, at the entrance into the Tyrrhenian Basin, the vein is found to flow deeper than 800 m.

In general, the evolution of the hydrographic characteristics of EMDW from its entry to the strait to the

TABLE 3. As for Table 1 but relative to the MATER 2 cruise (Fig. 4). In addition, the entrainment parameter $E^* \equiv 0$. This unrealistic result underlines the efficacy of intermittent velocity jumps in mixing these water masses. Indeed, the Baringer and Price (1997a,b) estimate of E^*, as described by (16), gives more realistic E^* values. These last estimates are finally used in the main entrainment equation (17) as a check on the effectiveness of our E^* values: here $\Delta\phi_{EMDW}$ is the alongstream variation of the EMDW flux.

	Section						
	I	II	III	IV	V	VIc	VII
g' (10^{-4} m s^{-2})	3	3	4	6	6	3	2
σ_{bottom}	29.168	29.165	29.163	29.157	29.150	29.124	29.117
h (m)	120	150	140	100	50	150	200
b (m)	550	600	800	530	350	600	1200
dist (km)	80	135	170	25	65	25	
W (km)	20	80	40	15	15	30	20
$\mathcal{A}_{EMDW}$ (km^2)	1.7	3.2	4	1.5	0.7	2.3	2.2
$\mathcal{A}_{LIW}$ (km^2)	16	40	62	5.0 + 2.2*	1.3 + 12.5*	18	30
V_2 measured (cm s^{-1})				18 and 51*	53 and 10*		
ϕ_{LIW} (Sv)				2.0	1.9		
V_2 (cm s^{-1})	12	5	3.2	18	53	11	7
$U \equiv V_2 + (U - V_2)$ (cm s^{-1})	13.5	8	5	14	46	15	17
ϕ_{EMDW} estimated (Sv)	0.23	0.26	0.2	0.23	0.32	0.35	0.34
Fr $= \lvert U - V_2\rvert/\sqrt{g'h}$	0,1	0,2	0,1	0,2	0,8	0,2	0,5
$E^*_{\text{Baringer Price}}(10^{-4})$	0	10^{-5}	10^{-4}	2×10^{-4}	9×10^{-4}	3×10^{-4}	/
$\Delta\phi_{EMDW} = \lvert U - V_2\rvert W E^*$dist ($10^{-4}$ Sv)	/	8	2	2	5	68	9

* This value corresponds to the Sicilian-side passage of sections IV and V (Fig. 1), which is crossed only by LIW water. Note that E^*_{Turner}, the entrainment computed following Turner's estimate, is zero.

Tyrrhenian Sea (Fig. 4b) shows a gradual increase both in temperature and in salinity, which corresponds to a progressive lightening of EMDW from section I (eastern sill) to section IV, indicative of rather weak mixing processes. This change is particularly evident between sections IV and VI. Between IV and V this is probably due to the topographic blocking effect of the sill, which permits only the passage of the upper part of the vein, and between V and VI it is due to the strong mixing. The current measurements available at the western sill (positioned in sections IV and V at about 125 m and 20 m from the sea bottom, respectively) indicate that the current is always running westward at a mean velocity of 18 and 53.2 cm s^{-1}, respectively; the maximum observed values are 38 and 67 cm s^{-1} in sections IV and V, respectively. From Table 3 we can also observe the maximum density reached by the vein: the vein enters the Malta sill with $\sigma_\theta \sim 29.168$, crosses the western sill with a value of $\sigma_\theta \sim 29.152$, and reaches the Tyrrhenian Basin with $\sigma_\theta \sim 29.117$, very close to buoyant equilibrium with the resident water. The geometric parameters of the vein do not change significantly along the strait either: the most significant changes are at the western sill (section V).

d. MATER 4 (May 1998)

The same measurements were repeated during the spring period of 1998. The vein is heavier than during the previous cruise along the whole channel, even if it reaches the same density at the entrance to the Tyrrhenian Basin (Fig. 5a). Also in this case the isopycnal slope is the same as that of MATER 2. Also of interest is the new section IIIa (Pantelleria Island), where the same general behavior as detected in sections IV and V is found. Thus, the ''anomaly'' in the isopycnal slope is not confined to the western sill region but begins earlier when the bottom becomes narrower (Fig. 1). The θ–S characteristics confirm the previously observed behavior. In terms of current dynamics in this period velocities, and the corresponding fluxes, are ~30% smaller than those observed during January 1997 (Table 4).

In a preliminary synthesis, the vein monitoring over the different seasons and years may be said to indicate that the presence of dense water is a quasi-permanent feature of the region. The dense water vein, deeply constrained by the topography, displays almost the same trajectory as it crosses the strait and reaches the Tyrrhenian Sea (Fig. 6). The vein enters the eastern sill and sinks to a depth greater than 800 m. It later rises to less than 300 m before definitively sinking to more than 1000 m. All measurements agree in showing almost stable characteristics of the vein as far as the western sill. So the most interesting region corresponds to the western sill and immediately downstream from it (sections IV–VI). It is important to observe that in this region, characterized by two distinct passages (Fig. 1), the vein flows through the Tunisia-side passage. Also significantly stable are the hydrographic characteristics during all the periods examined, while the current intensity and the associated flux seems to be more energetic during the cold season, as is usual in the Mediterranean Sea.

3. The model of multilayer steady flows in a strait

The above described features are general enough to encourage a theoretical discussion on the dynamics of a bottom current flowing steadily along a rather regular

marine strait, under some other moving layers. The sea bottom $b(x, y)$ is such that $\partial b/\partial x \ll \partial b/\partial y$. Here $x(y)$ is the alongstrait (cross-strait) coordinate; the interfaces among the various layers are $H_i + h_i(x, y, t)$, with $H_i =$ const. The corresponding hydrostatic pressure field is

$$\begin{aligned} p_1 &= p_0 + g\rho_1(h_1 - z) \quad \text{in the upper layer,} \\ p_2 &= p_0' + g\rho_2(h_2 - z) + g\rho_1(h_1 - h_2) \\ &\qquad \text{in the second layer,} \\ p_3 &= p_0'' + g\rho_3(h_3 - z) + g\rho_2(h_2 - h_3) + g\rho_1(h_1 - h_2) \\ &\qquad \text{in the third layer} \end{aligned} \tag{1}$$

with p_0, p_0', p_0'' constant. In the cross-strait direction the interface slopes $\partial h_1/\partial y = \gamma_1$ are approximately uniform across the strait (Fig. 7a). Consequently, assuming densities and velocities homogeneous inside each layer from (1), the geostrophic balance (Gill 1977; Salusti and Travaglioni 1985) gives

$$\begin{aligned} fV_1 &= \gamma_1 g \\ fV_2 &= \gamma_2 g\left(\frac{\rho_2 - \rho_1}{\rho_2}\right) + \frac{\rho_1}{\rho_2} fV_1 \simeq \gamma_2 g\left(\frac{\rho_2 - \rho_1}{\rho_2}\right) + fV_1 \\ fV_3 &= \gamma_3 g\frac{\rho_3 - \rho_2}{\rho_3} + \frac{\rho_2}{\rho_3} fV_2 \\ &\simeq \gamma_3 g\left(\frac{\rho_3 - \rho_2}{\rho_3}\right) + fV_2, \end{aligned} \tag{2}$$

where f is the Coriolis parameter and V_i the geostrophic alongchannel velocities. It has to be stressed that, if the sea bottom $b(x, y)$ is not particularly regular, a deflection and a centrifugal force have also to be considered. Consequently (2) holds as long as $fV_n \gg V_n^2/R_n$, these R_n being the internal radii of curvature of the various layers.

For the inviscid case the alongstrait equations of motion and the corresponding Bernoulli functions are

$$\left.\begin{aligned} &\text{in the upper layer:} \\ &\frac{\partial}{\partial t}V_1 + \frac{\partial}{\partial x}B_1 = 0, \qquad B_1 = \frac{1}{2}V_1^2 + gh_1 \\ &\text{in the second layer:} \\ &\frac{\partial}{\partial t}V_2 + \frac{\partial}{\partial x}B_2 = 0, \qquad B_2 = \frac{1}{2}V_2^2 + gh_2 + g\rho_1/\rho_2(h_1 - h_2) = \frac{1}{2}V_2^2 + g\frac{\rho_2 - \rho_1}{\rho_2}h_2 + g\frac{\rho_1}{\rho_2}h_1 \\ &\text{in the third layer:} \\ &\frac{\partial}{\partial t}V_3 + \frac{\partial}{\partial x}B_3 = 0, \\ &\qquad B_3 = \frac{1}{2}V_3^2 + gh_3 + g\rho_2/\rho_3(h_2 - h_3) + g\frac{\rho_1}{\rho_3}(h_1 - h_2) = \frac{1}{2}V_3^2 + g\frac{\rho_3 - \rho_2}{\rho_3}h_3 + g\frac{\rho_2 - \rho_1}{\rho_3}h_2 + g\frac{\rho_1}{\rho_3}h_1. \end{aligned}\right\} \tag{3}$$

Note that in the inviscid time-independent case equations (3) correspond to (Lane-Serff et al. 2000)

$$\begin{aligned} \frac{\partial}{\partial x}B_1 &= \frac{\partial}{\partial x}\left[\frac{1}{2}V_1^2 + gh_1\right] = 0 \\ \frac{\partial}{\partial x}\left(B_2 - \frac{\rho_1}{\rho_2}B_2\right) &= \frac{\partial}{\partial x}\left[\frac{1}{2}V_2^2 + g\frac{\rho_2 - \rho_1}{\rho_2}h_2 - \frac{\rho_1}{\rho_2}\frac{1}{2}V_1^2\right] = 0 \\ \frac{\partial}{\partial x}\left(B_3 - \frac{\rho_2}{\rho_3}B_3\right) &= \frac{\partial}{\partial x}\left[\frac{1}{2}V_3^2 + g\frac{\rho_3 - \rho_2}{\rho_3}h_3 - \frac{\rho_2}{\rho_3}\frac{1}{2}V_2^2\right] = 0. \end{aligned} \tag{4}$$

Interestingly, these equations show how the kinetic energy of the ith layer plays an important role in the dynamics of the lower $(i + 1)$th layer but with an opposite sign, the classical Bernoulli suction.

Now B_i are no longer constant along a streamline if friction and mixing are to be taken into account. Calling $\rho_i\mathcal{M}_i$ the total effect of these stresses on the ith layer, the equations of motions (3), now integrated over a cross section of a layer of area $\mathcal{A}_i$, give

$$\mathcal{A}_i\frac{\partial}{\partial t}V_i + \mathcal{A}_i\frac{\partial}{\partial x}B_i = \mathcal{M}_i \tag{5}$$

since we assumed that velocities, densities, etc., can be considered as homogeneous inside each layer. Note that the terms $\mathcal{M}_i$, here assumed to act into the layer below the interface, are essentially retarding the currents. In addition, these stresses are mainly localized in the upper and lower viscous boundaries of each layer, so it is probably more realistic to consider V_i, ρ_i, etc., as averages over a cross section of these quantities, as in classical stream-tube models (Smith 1975; Killworth 1977). Note also that these relations are general but for

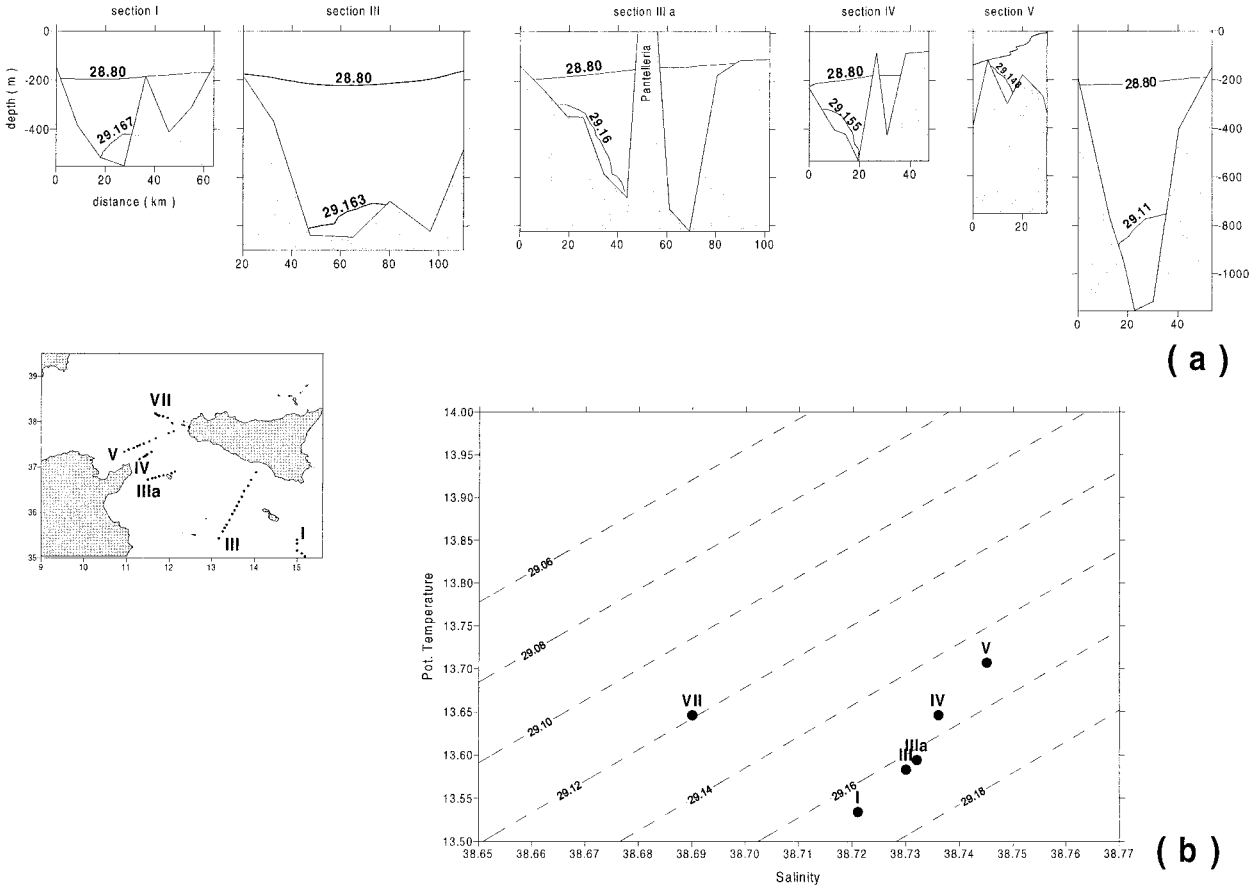

FIG. 5. As in Fig. 2 but for MATER 4 cruise (21 Apr–14 May 1998).

the lowest layer the interaction of the current with the bottom has to be considered.

In conclusion, the steady equations (4) now become

$$\mathcal{A}_i \frac{\partial}{\partial x}\left(\frac{1}{2}V_i^2 + g\frac{\rho_i - \rho_{i-1}}{\rho_i}h_i - \frac{1}{2}\frac{\rho_{i-1}}{\rho_i}V_{i-1}^2\right) = \mathcal{M}_i - \frac{\rho_{i-1}}{\rho_i}\frac{\mathcal{A}_i}{\mathcal{A}_{i-1}}\mathcal{M}_{i-1}, \quad (6)$$

which, explicitly developed in appendix A for the Strait of Sicily, will be further discussed in the following.

4. The stream-tube model

As far as the lowest layer dynamics are concerned, even explicitly taking into account friction and mixing, a steady model that parallels recent studies by Emms (1997) and Baringer and Price (1997a,b) on density currents in a still environment will be now discussed. We consider incompressibility, downstream momentum and across-stream momentum for a steady flow, not under motionless layers but under two steady currents of different densities flowing in opposite directions, as in the Mediterranean case discussed above. In more detail, the EMDW is assumed to be a steady current of dense fluid, symmetrical about its centerline, identified by the streamwise coordinate ξ and with almost negligible variations in the across-stream direction ψ (Fig. 7b). The model equations are derived by introducing a transformation in a streamwise coordinates system (ξ, ψ) that makes an angle β with the usual (x, y) coordinates, and then space averaging over a cross section of the current (Smith 1975; Killworth 1977; Emms 1997). This idealization may appear rather crude, in particular when R_n is small, but affords good insight into these complex dynamics.

If the thickness of the bottom current is $h(\xi)$ and the average alongvein fluid velocity is $U(\xi)$, then for a small angle β incompressibility implies

$$\frac{\partial}{\partial \xi}\int hU\, d\psi = \frac{\partial}{\partial \xi}(\mathcal{A}U) = \mathcal{E} = E^*|U - V_2|W, \quad (7)$$

where $\mathcal{A} = \int h\, d\psi$ is the bottom current cross-sectional area, W is the current width, and $\mathcal{E}$ represents the total entrainment between the dense cold current and the upper layer of LIW, the velocity of which is V_2.

Entrainment has been extensively discussed in Ellison and Turner (1959), Turner (1986), and others. A par-

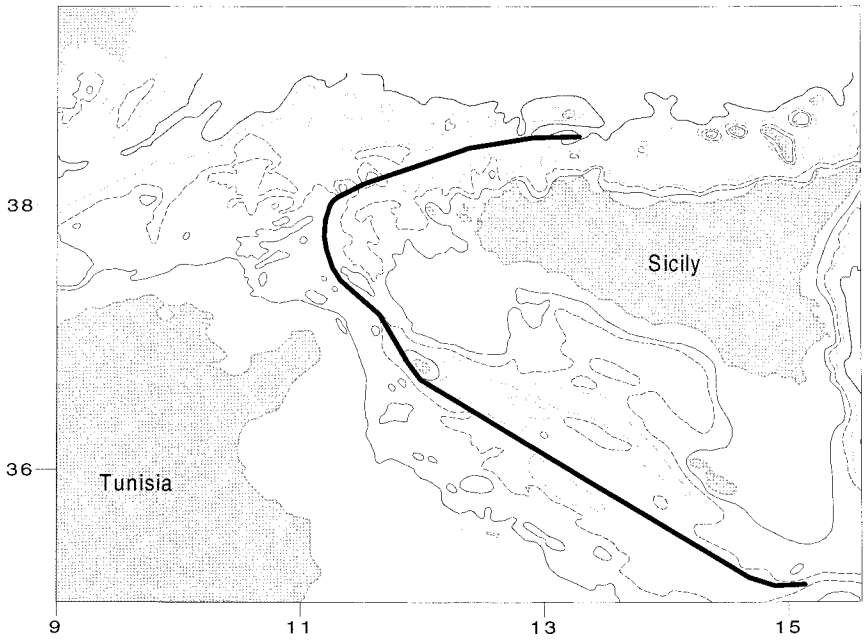

FIG. 6. Schematic route of the vein from the eastern boundary of the strait to the Tyrrhenian Sea. This trajectory corresponds to the centerline of the vein in the different hydrographic sections.

ticularly simple idealization has been chosen in (7), namely $\mathcal{E} = E^*|U - V_2|W$, where the entrainment rate E^* is assumed to be constant, and U and V_2 are the deepest layer velocities, here considered as almost parallel. More generally, E^* can be taken as a function of the Froude number

$$F = \sqrt{\frac{(U - V_2)^2}{g'h}}, \tag{8}$$

namely

$$E^* = \begin{cases} 0 & \text{for } F \le 1.25 \quad \text{(subcritical flow)} \\ \dfrac{0.08F - 0.1}{5 + F^2} & \text{for } F > 1.25 \quad \text{(supercritical flow).} \end{cases}$$

For the Mediterranean its efficacy will be discussed in the following.

Denoting the bottom current density as $\rho(\xi)$, for small β conservation of mass gives

$$\frac{\partial}{\partial \xi}(\rho \mathcal{A} U) = \rho_e(z)\mathcal{E} = \rho_e(z)E^*|U - V_2|W, \tag{9}$$

where $\rho_e(z)$ is the local environmental density, eventually depending on the depth z. Note how similar relations hold for any tracer present in the sea water.

The total downstream steady momentum is assumed to be balanced by friction, mixing, and the hydrostatic pressure gradient. Thus, incompressibility (7) and the conservation of momentum give

$$\frac{\partial}{\partial \xi}\left(U^2\mathcal{A} + g'\mathcal{A}\left[b + \frac{h}{2}\right]\right) = -\frac{WF_s}{\rho} - fV_2\mathcal{A}\sin\beta + \mathcal{D}\cos\beta, \tag{10}$$

where b is the bottom depth, h the thickness of the vein, and $F_s = \rho K U^2$ is the bottom drag. The first term in Eq. (10) combines the incompressibility (7) and the kinetic energy (Smith 1973, appendix A). The second term is the baroclinic pressure term, which accounts for changes in the hydrostatic pressure due to variations in buoyancy of the mean height of the vein, $b + h/2$. In early density current models this term was often disregarded, although Emms (1997) notes that near the edges of the current (Whitham 1955), and over sharp topographic features, this hydrostatic pressure term must be included in the bottom layer dynamics to balance the frictional term at the current head, as also done by Baringer and Price (1997a,b).

In (10) the term $\mathcal{D}$ takes into account the alongstrait hydrostatic pressure field acting on the vein, due to the overlying layers. If friction and entrainment are small, $\mathcal{D}$ is simply the Bernoulli suction

$$\frac{\rho_2}{\rho_3}\frac{1}{2}\frac{\partial}{\partial \xi}(\mathcal{A}V_2^2) \simeq \frac{1}{2}\frac{\partial}{\partial \xi}(\mathcal{A}V_2^2)$$

as discussed by Lane-Serff et al. (2000). For realistic cases where mixing and friction are important, as

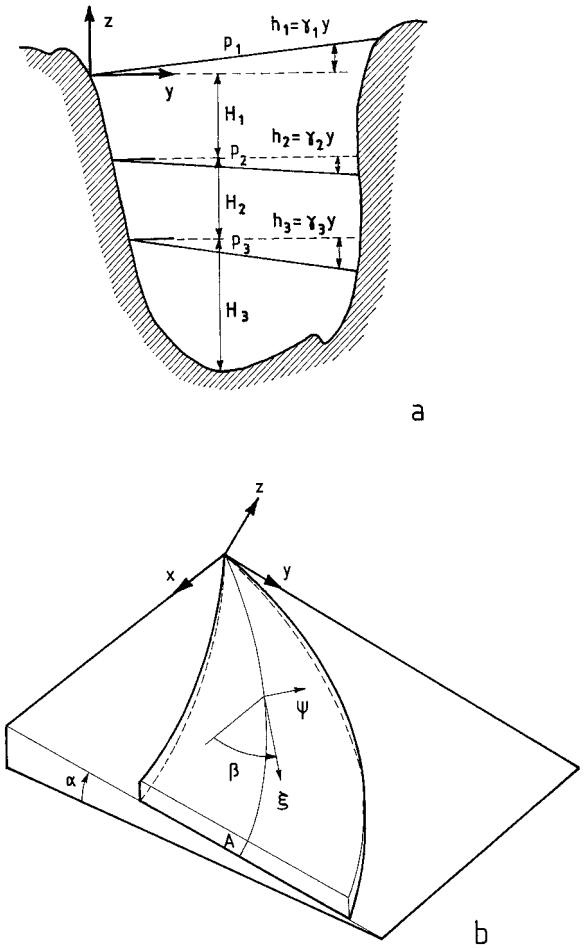

FIG. 7. (a) Schematic representation of the three-layer geostrophic situation. The layer boundaries are at $z = H_1 + h_1 = H_1 + \gamma_1 y$ for $H_i = \text{const}$, $z = H_2 + h_2 = H_2 + \gamma_2 y$, and $z = H_3 + h_3 = H_3 + \gamma_3 y$. In this sketch $\gamma_1 > 0$, $\gamma_2 < 0$, and $\gamma_3 < 0$ to simulate the situation described in the text. (b) Coordinate system of the model; the symbols are as explained in the text.

shown in appendix A, we have that for the deepest layer

$$\mathcal{D} = E^*W(U - V_2)^2 + \frac{\rho_2}{\rho_3}\left\{\frac{\partial}{\partial\xi}\frac{1}{2}V_2^2\mathcal{A} - \mathcal{A}\frac{\mathcal{M}_2}{\mathcal{A}_2}\right\}$$

$$\simeq E^*W(U - V_2)^2 + \frac{\partial}{\partial\xi}\frac{1}{2}V_2^2\mathcal{A} - \frac{\mathcal{A}\mathcal{M}_2}{\mathcal{A}_2} \qquad (11)$$

with $\mathcal{M}_2 = E'W(V_2 - V_1)^2 - E^*W(U - V_2)^2$.

Note also how the preceding relations (9)–(11) hold for a narrow channel, while the stream-tube models are valid under rather different conditions such as the flow being a narrow turbulent vein in a hydrostatic pressure field, moving over a regular mild slope, as fully discussed by Smith (1973). So the validity of (9)–(11) has to be checked in each practical case.

In addition it has to be stressed that, like the Bernoulli suction for inviscid fluids, friction and mixing in the upper layer play an important role in the dynamics of the lower-layer alongstream momentum, also in this case with opposite sign. Consequently these retarding effects for MAW and LIW actually accelerate the EMDW current (appendix A).

Finally, we equate the effect of the cross-stream component of gravity perpendicular to the direction of flow, the upper-layer hydrostatic pressures, and the Coriolis force to give

$$U^2\partial\beta/\partial\xi + fU + \frac{\partial}{\partial\psi}[g'(h + b)]$$

$$= fV_2\cos\beta + \mathcal{D}\sin\beta. \qquad (12)$$

Note in this equation the presence of

$$fV_2\cos\beta + \mathcal{D}\sin\beta$$

synthesizing the pressure effect of the cross-stream steady currents flowing over the vein (Emms 1997). In addition, centrifugal effects $U^2\partial\beta/\partial\xi$ can be disregarded if the deflection radius R_n is such that $fU \gg U^2\partial\beta/\partial\xi = \pm U^2/R_n$.

5. The diagnostic model of the bottom current in the Strait of Sicily

Now we focus our attention exclusively on incompressibility and steady momentum conservation, while (9) will be used in the following to discuss entrainment. Since $\partial b/\partial x \ll \partial b/\partial y$, as one would expect for regular sea bottom, for small β we have

$$\frac{\partial b}{\partial\psi} \simeq \frac{\partial b}{\partial y}\cos\beta \sim \frac{\partial b}{\partial y}[1 + \partial(\beta^2)] \sim \frac{\partial b}{\partial y} \qquad (13)$$

and consequently the error, of the order of β^2, can be considered small. This finally gives for $\beta \sim 0$ that

$$\frac{\partial}{\partial\xi}(\mathcal{A}U) = E^*|U - V_2|W \qquad (14a)$$

$$\frac{\partial}{\partial\xi}[U^2\mathcal{A} + g'\mathcal{A}(h/2 + b)] + KWU^2 - \mathcal{D} = 0 \qquad (14b)$$

$$f(U - V_2) + g'\frac{\partial}{\partial y}(h + b) = 0. \qquad (14c)$$

It is interesting to note how, formally, the third equation becomes the classical thermal wind equation.

Equations (14a–c) can be discussed perturbatively, as in appendix B, but in the following will be used to diagnose our dataset in order to gain some insight into the Strait of Sicily cold dense water dynamics. Generally, at the sill, the LIW velocity V_2 is larger than the lowest layer velocity U. Therefore, the cold dense current cannot flow near the Sicilian coast, but is pushed toward the African coast by the energetic LIW current. But farther west, where the channel is wider, V_2 weakens and at a certain distance from the sill it is U that becomes

larger than V_2. The dense cold water can thus reach the deepest bottom layer and then start flowing in accordance with the geostrophic relations. This can explain the deepening and the subsequent crossing of the sill midline by the dense cold current. Note how this is actually a geostrophic motion that, under the effect of the upper-layer velocities, can also appear as ageostrophic.

In practice, in the following paragraphs we first identify the position of EMDW and its center in the various hydrographic sections. This allows us to identify its trajectory and consequently the angle β. From the cross-strait geostrophic balance the importance of the centrifugal effects $U^2\partial\beta/\partial\xi$ can thus be estimated, as well as the reliability of the $\beta \sim 0$ approximation. Once the effect of β is determined, from the hydrographic properties of EMDW and LIW in the various sections the cross-sectional areas $\mathcal{A}_{\text{LIW}} = \mathcal{A}_2$ and $\mathcal{A}_{\text{EMDW}} = \mathcal{A}$ can be obtained and, using continuity, also the velocities V_2 can be estimated. The thermal wind equation then gives U in the various sections. Finally the alongstrait momentum allows us, as in Baringer and Price (1997a,b), to analyze the various physical mechanisms that rule the EMDW dynamics, namely entrainments, friction, and alongstrait pressure fields. In the end we also discuss if this stream-tube model can reasonably be applied to analyzing the deep EMDW current dataset.

6. Comparison with observations in the Strait of Sicily

Since the PRIMO and MATER 1 cruises do not concern the eastern mouth of the Strait of Sicily, we chose to present only the datasets of the MATER 2 and 4 cruises in light of the previous model. This will allow us to compare model results and data in this two-sill system and verify the model behavior in different rising and sinking situations of the vein.

a. MATER 2 cruise

Data collected during the MATER 2 cruise in the Strait of Sicily (Jan 1997) are now compared with model results. The various sections are located as shown in Fig. 4; the bottom topography far from the sill is comparatively regular but the sill topography is particularly complex, with some deep canyons (Fig. 1). In Table 3 we have also resumed the most important data relative to the seven sections of the MATER 2 cruise.

Let us first consider the cross-strait balance. The bottom current of EMDW is easily identified in each section. Consequently, $g' \equiv g(\rho_{\text{EMDW}} - \rho_{\text{LIW}})/\rho_{\text{LIW}}$ and σ_θ on the sea bottom are determined (Table 3). It is worth noting that σ_θ on the sea bottom is constantly decreasing westward, from section I to section VII. This clearly shows that EMDW is gradually mixing with LIW in its westward travel and justifies the absolute value in Eqs. (7) and (9). Also of interest is the fact that the deflection angle β is very small in most sections; in the westernmost sections (IV–VI) we have that $\beta \neq 0$ and $(\partial\beta/\partial\xi)^{-1} \sim 40$ km rad^{-1} (Fig. 6). Since the averaged values of the bottom velocities are about 10–20 cm s^{-1}, the centrifugal effects are $U^2\partial\beta/\partial\xi \sim (3\text{–}12) \times 10^{-7}$ m s^{-2}, while $fU \sim (1\text{–}2) \times 10^{-5}$ m s^{-2}: in the following we assume $\beta \sim 0$ without fear of serious errors.

Now, on comparing the continuity equation (14a) with our data, a more complex situation is seen to emerge. First we estimate $\mathcal{A}_{\text{EMDW}}$ and $\mathcal{A}_{\text{LIW}}$, the cross-section areas for these currents. Then we use the (few) available current meter data to obtain the flux of LIW, namely $\phi_{\text{LIW}} \sim 1.9$ Sv (Sv $\equiv 10^6$ m^3 s^{-1}) from the data of section IV. From section V data we have $\phi_{\text{LIW}} \sim 2$ Sv. Table 3 also shows the corresponding LIW velocities V_2, computed using continuity, the velocities U, using the thermal wind equation, and the corresponding EMDW flux $\phi_{\text{EMDW}} \sim 0.23$ Sv (at the eastern boundary of the strait, sections VI and V) and ~0.37 Sv (at the western boundary, section VII).

We can now estimate $\mathcal{E}$. Better, we have two different ways of estimating the entrainment of EMDW. The first is inferred from classical tank experiments (Turner 1986): essentially entrainment, ruled by the Froude number, is

$$E^* = \begin{cases} 0 & \text{for } F \leq 1.25 \quad \text{(subcritical flow)} \\ \dfrac{0.08F - 0.1}{5 + F^2} & \text{for } F > 1.25 \quad \text{(supercritical flow).} \end{cases} \tag{15}$$

Since in this strait $\sqrt{g'h} \sim 10\text{–}20$ cm s^{-1} is larger than $|U - V_2|$, these flows are subcritical. Only over section V does the Froude number approach 1, so from (15) everywhere $E^* \sim 0$. However, current meter data show large velocity variations (Astraldi et al. 1996), so an intermittent E^* can easily attain large values, even if the average velocity corresponds to $E^* \sim 0$. To check this last possibility we computed E^* empirically using volume and mass conservation, as fully discussed in Baringer and Price (1997b). This essentially consists of considering both equations (7) and (9), which give

$$\mathcal{A}U\frac{\partial\rho}{\partial\xi} = \mathcal{E}^*(\rho_e - \rho) \simeq E^*W|U - V_2|(\rho_e - \rho), \tag{16}$$

namely a model way of estimating E^* once ρ, U, W, V_2, $\mathcal{A}$ are known with reasonable accuracy. It would be natural to consider also salinity conservation, but the existing salinity data showed less significant variations, so density was ultimately used. The computed E^* are in Table 3; a reasonable synthesis is that $E^* \sim 10^{-5}$ east of the sill and $E^* \sim 10^{-3}$ on the sill, which are not surprising estimates. In addition these values are in substantial agreement with the original entrainment idea of alongstrait increase of EMDW flux,

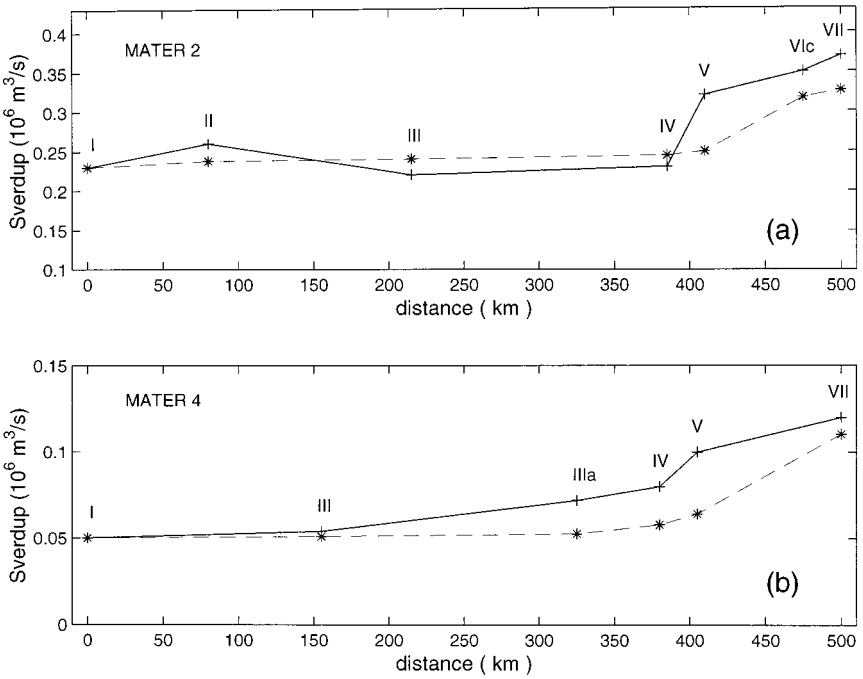

FIG. 8. Evolution of vein flux from the eastern sill toward the Tyrrhenian Sea: comparison between the model results (dashed line) and in situ data (continuous line). Roman numerals indicate the section numbers for the (a) MATER 2 cruise and (b) MATER 4 cruise.

$$\phi_{\mathrm{EMDW}} = \phi^0_{\mathrm{EMDW}} + \int_0^{\xi} d\xi' E^*(\xi')|U - V_2|W(\xi'), \quad (17)$$

as can be seen by analyzing Table 3. Here ϕ_{EMDW} is the alongstream flux of EMDW, while ϕ^0_{EMDW} is the same flux in section I. In more detail, the reconstructed flux values using (17) have the correct trend but appear somewhat small, even taking into account that such flux estimates often show large approximations (Fig. 8a).

Finally, we use this value E^* by assuming, as in Baringer and Price (1997b), that the total entrainment stress between LIW and EMDW is

$$\rho E^*(U - V_2)^2 W. \quad (18)$$

Since LIW and EMDW are both flowing westward, we finally obtain a rather small stress, which is analyzed in more detail in the following.

We can now discuss alongstrait momentum conservation (14b). The situation is again substantially different in the regions east and west of section V, the western sill. Indeed in the eastern part EMDW is found at a depth of 300–800 m, while over the sill it is at 220–350 m. Farther west, EMDW is at a depth of 900–1000 m. It is thus evident that there is some forcing that pushes the dense EMDW vein toward the sill. The most natural dynamical candidates are the alongstrait pressure gradients that push the bottom water toward the sill, unlike the bottom friction which is always retarding the current. These two effects are opposite in the eastern part of the strait, but they concur in the western part. In conclusion, since in this strait friction and mixing cannot be disregarded, the term $\mathcal{D}$ as formulated in (11) must be considered.

Estimates of the various forcings are shown in Fig. 9a. It is first evident that the EMDW "kinetic energy" $\mathcal{K} = U^2\,\mathcal{A}$ and Bernoulli suction $\mathcal{B} = 1/2\mathcal{A}V_2^2$ are rather regular functions, but with opposite signs that in (14b) essentially compensate each other (Baringer and Price 1997a,b). The potential energy is strongly related to the alongflow bottom topography: from east to west, it first decreases starting from the eastern sill, then increases toward the western sill, and finally decreases sharply on arriving at the southern Tyrrhenian Sea. The evolution of the alongstream gradients of the previous quantities (Fig. 9b) indicate that they must be compensated for by bottom friction, a retarding quantity, and by the upper-layer friction and mixing. But since LIW and EMDW both flow westward, it is ultimately the stress between MAW and LIW that plays a fundamental role in $\mathcal{D}$. Indeed the entrainment stress between LIW and EMDW, because of the small velocity differences $|U - V_2|$, is a very small quantity. Consequently, it is essentially the interfacial stress between MAW and LIW $\sim E'(V_1 - V_2)^2 W$ that is large, especially in the sill region where $|V_1 - V_2| \gtrsim 40$ cm s^{-1}. If one assumes a realistic MAW–LIW entrainment parameter E' to account for the numerous exchanges of mass and energy between the two major basins of the Mediterranean Sea, then this interfacial stress can be estimated.

Note that the overall result of the strong MAW–LIW

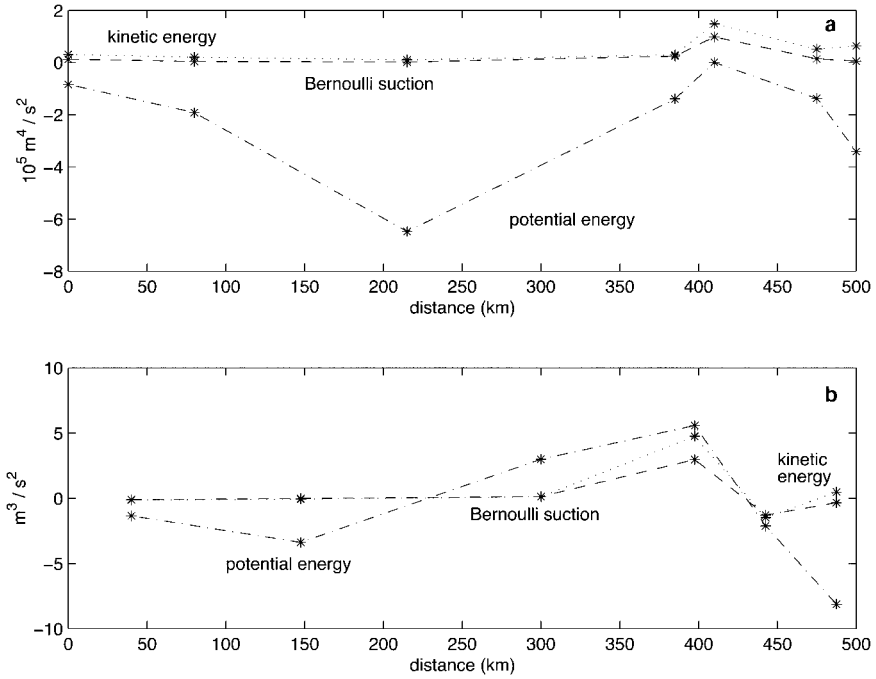

FIG. 9. MATER 2 alongstream momentum balance: (a) ''kinetic energy'' $\mathcal{K}$ (dotted line), Bernoulli suction $\mathcal{B}$ (dashed line), and potential energy (dot–dashed line). (b) Alongstream derivative of the previous terms.

interaction and of the milder LIW–EMDW interaction is a strong accelerating forcing on EMDW toward the west, essentially localized in the narrow sill region. And this allows us to use (11) without fear of serious errors.

So, from the preceding analysis (see also appendix A) we finally obtain the explicit formulation of (14b) for the Strait of Sicily, namely

$$\frac{\partial}{\partial \xi}\left(U^2\mathcal{A} + g'\mathcal{A}[h/2 + b] - \mathcal{A}\frac{1}{2}V_2^2\right) - E^*W(U - V_2)^2 + \frac{\mathcal{A}}{\mathcal{A}_2}[E'W(V_2 - V_1)^2 - E^*W(U - V_2)^2] + KWU^2 = 0. \quad (19)$$

Using the previous value of $E^* = 10^{-4}$, a reasonable estimate of $E' = 3.2 \times 10^{-2}$ and $K = 2.6 \times 10^{-2}$ can be obtained applying a linear regression (Fig. 10) between alongstream gradient terms and stress terms of Eq. (19). The alongstream evolution of these stress terms, together with the resultant total stress (Fig. 11a), indicates that $E'(V_2 - V_1)^2$ is comparable with the bottom stress, while the total stress is smaller. Finally Fig. 11b shows a good balance between alongstream momentum gradients and total stresses, as estimated from the experimental data.

b. MATER 4 cruise

We now repeat the previous discussion on the MATER 4 data (May 1998), paralleling those obtained during the MATER 2 cruise. The main results are summarized in Table 4. Concerning the EMDW cross-strait balance, the midline shown in Fig. 6 is practically equivalent to that observed during the MATER 2 cruise, so, also in this case, we can assume $\beta \sim 0$. Interestingly g' and σ_θ are also quite similar to those of the MATER 2 cruise. A similar trend can be observed for the flux of LIW: from sections IV and V we have a LIW flux that can reasonably be estimated as $\phi_{\mathrm{LIW}} \sim 1.2$ Sv. We tentatively assume this value to be constant throughout LIW's travel through the strait, in order to obtain an estimate of the LIW velocity V_2 from continuity.

The EMDW velocity U is thus obtained using the

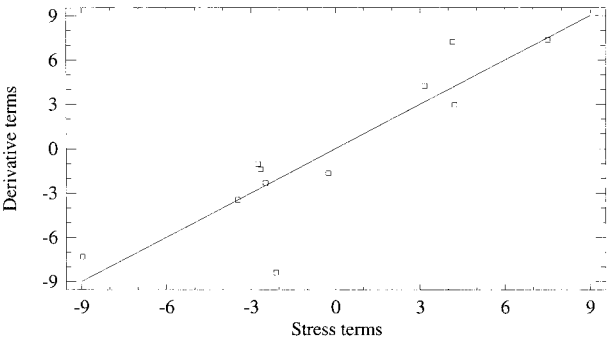

FIG. 10. Bivariate linear regression between the alongstream derivative terms and stress terms of (19), assuming $E^* = 10^{-4}$: we finally obtain $E' = 3.2 \times 10^{-2}$ and $K = 2.6 \times 10^{-2}$. Experimental data of both MATER 2 and MATER 4 have been used (Tables 3 and 4).

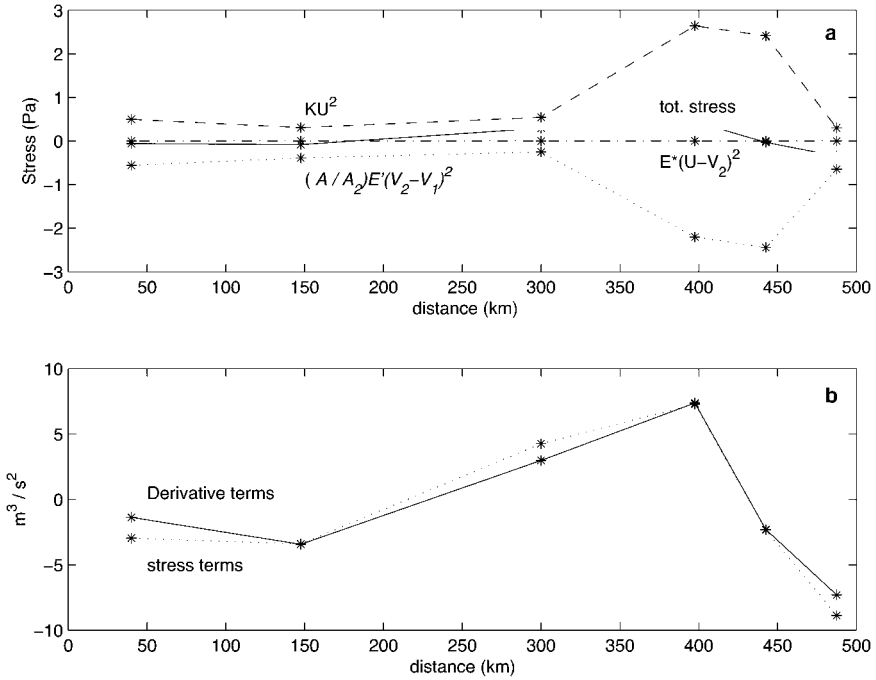

FIG. 11. MATER 2 data (a) components of Tables 3 and 4 bottom stress KU^2 (dashed line), LIW–EMDW entrainment stress (dot–dashed line), MAW–LIW entrainment stress $E'\mathcal{A}_2^{-1}\mathcal{A}(V_2 - V_1)^2$ (dotted line), and resulting total stress (continuous line). (b) Alongstream derivative terms (continuous line) and their resultant, namely the stress terms (dotted line), as in (19).

thermal wind equation, and the resulting ϕ_{EMDW} is ~0.06 Sv at the eastern mouth of the strait, while at its western exit it is higher, $\phi_{\text{EMDW}} \sim 0.08$ Sv at section V and 0.12 Sv in the last section, VII (Table 4).

In general, in this dataset the velocities, stratifications, etc., have trends similar to those already described for the MATER 2 cruise but are less energetic, as is usual during spring for the Mediterranean Sea. Again, the Turner estimate of E^*, as in the MATER 2 cruise, is zero. The other Baringer and Price estimate gives $E^* \sim 10^{-4}$ far from the sill. It is larger, $E^* \sim 4 \times 10^{-3}$, near the sill. As a check, we also computed from Eq. (17) the evolution of the flux of EMDW namely $\Delta\phi_{\text{EMDW}}$ (Table 4), for the various sections, which is in reasonable agreement with the data (Fig. 8b). Finally, we again examined the role of friction and of $\mathcal{D}$. Repeating the

TABLE 4. As for Table 3 but for the MATER 4 cruise (Fig. 5).

	Section					
	I	III	IIIa	IV	V	VII
g' (10^{-4} m s^{-2})	8.3	8.2	8	7.8	7.4	6
σ_{bottom}	29.167	29.165	29.163	29.156	29.148	29.119
h (m)	75	125	100	50	25	130
b (m)	550	700	650	500	360	1150
dist (km)	155	170	60	25	90	
W (km)	15	5	22	15	8	18
$\mathcal{A}_{\text{EMDW}}$ (km^2)	0.4	0.9	2.4	1	0.4	1.7
$\mathcal{A}_{\text{LIW}}$ (km^2)	12	62	10	3.4 + 2.2*	1.2 + 12*	24
V_2 measured (10^{-2} m s^{-1})				13 and 34*	35 and 6*	
ϕ_{LIW} measured (Sν)				1.2	1.2	
V_2 (10^{-2} m s^{-1})	10	2	12	13	35	5
$U = V_2 + (U - V_2)$ (10^{-2} m s^{-1})	12	6	3	8	27	8
ϕ_{EMDW} (10^{-2} Sν)	5	5.4	7.2	8	10	12
$F_2\ \lvert U - V_2\rvert/\sqrt{g'h}$	0.1	0.05	0.3	0.2	0.6	0.03
$E^*_{\text{Baringer Price}}$ (10^{-4})	0.2	0.1	1.3	4	4.5	
$\Delta\phi_{\text{EMDW}} = \lvert U - V_2\rvert W E^*$dist ($10^{-4}$ Sν)		10	17	49	62	460

* This value corresponds to the Sicilian-side passage of sections IV and V (Fig. 1), which is crossed only by LIW water. Note that in this case also $E^*_{\text{Turner}} = 0$.

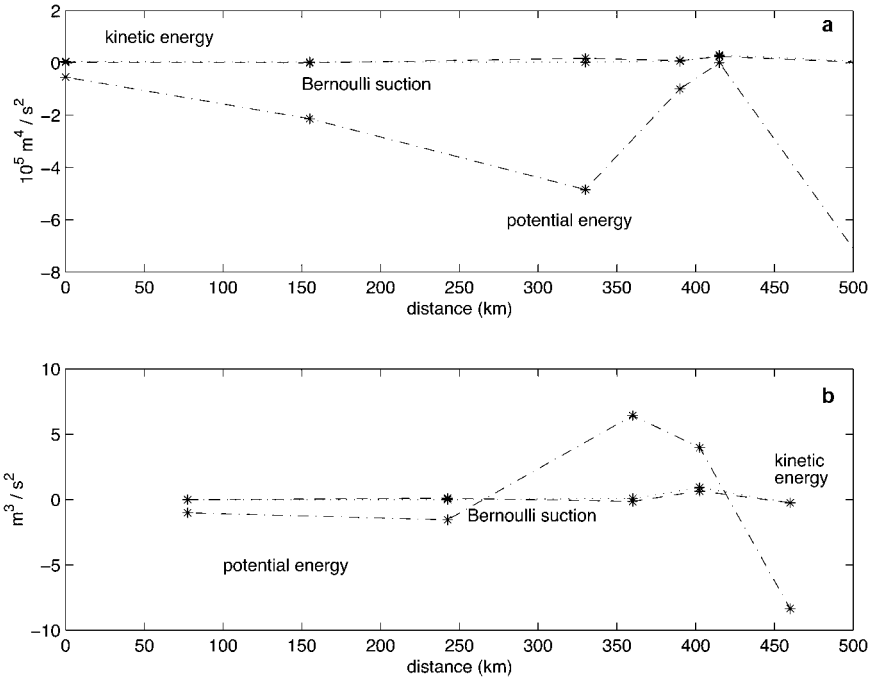

FIG. 12. MATER 4 alongstream momentum balance: (a) ''kinetic energy'' $\mathcal{K}$ (dotted line); Bernoulli suction $\mathcal{B}$ (dashed line), and potential energy (dot–dashed line). (b) Space derivatives of each of the previous terms.

estimates made for MATER 2, we obtained a similar behavior for the energy terms (Fig. 12a) and the alongstream derivatives in Eq. (19) as shown in Fig. 12b. Also for MATER 4 the evolution of stress terms along the vein trajectory (Fig. 13a) evidences the important role played by the MAW–LIW entrainment stress. The balance between alongstream derivatives and total stress (Fig. 13b) is however not as good as for MATER 2. This can be partially explained by the poor data coverage (if compared with the MATER 2 dataset) downstream of the western sill (Fig. 5), where the larger imbalance can be observed.

7. Conclusions and discussion

The observations made in the Strait of Sicily during different seasons evidence the presence of a quasi-steady current flowing westward directly over the bottom of the strait. It consists of a dense vein of EMDW that is able to cross the Malta sill, flows along the deep region of the strait, and finally outflows westward into the Tyrrhenian Sea. Due to its high density ($\sigma_\theta \sim 29.10$), when it reaches the Western Mediterranean basin it sinks, finding its neutral buoyancy at a depth of about 1500–1800 m. Interestingly, our data show that in each of the observational periods the geometric properties of the current (height, width, path) show only minor variations, a particularly intriguing observation. Some changes are observed in the θ–S properties, while the mean velocity values seem subject to a seasonal cycle. The stable behavior of the vein allows us to identify the main mechanisms responsible for its evolution and indicate the westward sill region (section V) as the site where the most noticeable changes in the vein properties and the most significant dynamic effects take place.

In this work we focused our attention especially on the peculiarities of the interface slope of the vein immediately upstream of the sill, and on evaluating the relative importance of stresses (bottom and entrainment), alongflow pressure gradients, and Bernoulli suction. Over most of its path, the vein closely follows the local bathymetry. Its trajectory inside the strait follows an almost straight line; its depth is ~550 m at the eastern entrance, increases slowly to about 800 m in the central part of the strait, and successively, in proximity of the western sill, its value is reduced to about 300 m. From the sill the vein starts to descend and at the same time turns east so that when it enters the Tyrrhenian Sea (section VII) its velocity is practically aligned along the Sicilian continental shelf slope, where it continues to sink to a depth of about 1800 m. This change of direction is in agreement with a cross-stream geostrophic balance.

The cross-stream momentum equation, taking into account also the dynamical effects of the circulation in the upper layers, demonstrates how deeply the latter can influence the vein evolution. More specifically, the position and slope of the vein at the western sill can be explained in terms of geostrophic balance: the presence of the vein along the Tunisian side is essentially due to the effect of the higher velocity of LIW compared with

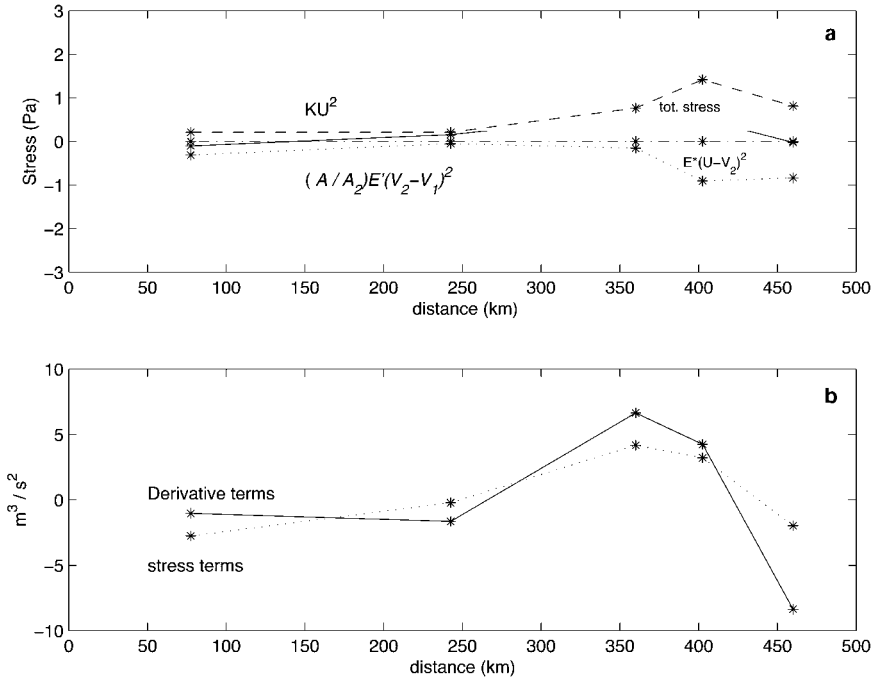

FIG. 13. MATER 4 data (a) components of bottom stress KU^2 (dashed line), LIW–EMDW entrainment stress (dot–dashed line), MAW–LIW entrainment stress $E'\mathcal{A}_2^{-1}\mathcal{A}(V_2 - V_1)^2$ (dotted line), and resulting total stress (continuous line). (b) Alongstream derivative terms (continuous line) and total stress (dashed line), as in (19).

the deep vein velocity. The diagnostic analysis of the alongstream momentum equation shows that the kinetic energy reaches a maximum at the western sill (section V). Taking this western sill as a reference, the potential energy has negative values both east and west of the sill. Farther east the elementary mechanism moving the vein toward the sill consists of the upper-layer pressure gradients, which are able to raise the vein from ~800 to 300 m depth, thus increasing both the potential energy and the kinetic energy to their highest values. Subsequently, we observe that a decrease of potential energy does not correspond to any kinetic energy increase but conversely, to a decrease, especially between sections V and VI. This underlines the important role played by stresses downstream of the western sill toward the Tyrrhenian Sea. The importance of entrainment downstream of the sill is also evident if we consider how the flux of this vein evolved during January 1997 (MATER 2): estimated as ~0.23 Sv at its entrance to the Malta sill, the flux maintains approximately the same value as far as section IV and increases considerably after the western sill, reaching 0.37 Sv when the vein enters the Tyrrhenian Basin. During April/May 1998 (MATER 4) the same flux, considerably weaker than January 1997, doubles its value from section I to section VII.

In summary, in this study we have documented the seasonal characteristics of the EMDW deep-layer dynamics in the Strait of Sicily, such as velocity field, forcings, fluxes, and interface evolutions. In addition, a critical version of geostrophic balances gives current velocities in good agreement with the data. The application of the classical stream-tube model (Smith 1973, 1975; Killworth 1977; Emms 1997; Baringer and Price 1997a,b), generalized by taking into account the effects of moving upper layers, LIW and MAW, evidenced the importance of the Bernoulli suction (Lane-Serff et al. 2000) and, more specifically, of the strong influence of MAW–LIW entrainment stress on the alongchannel pressure gradients, which finally push the deep vein through the western sill. Indeed, we show that, while the entrainment stress between LIW and EMDW has a rather negligible dynamical effect, the MAW–LIW stress has the same importance as bottom stress, deeply influencing the resulting total stress and allowing a considerable uplift of EMDW in the sill region. It is also interesting to remark that the entrainment stress between MAW and LIW, being of the same order of $1/2V_2^2$, also has an important effect on the dynamics of LIW over the sill.

The results obtained in the Strait of Sicily by applying the previous generalization of the Smith stream-tube model allows us to assert that, when we are in the presence of a multilayer system and there is a considerable velocity difference between the two layers immediately over the vein, its effect can be very important for the vein and therefore one has to take into account the dynamics of these layers.

It should also be noted how the stream-tube model

was applied here, in a certain sense outside its theoretical field of applicability. It should indeed be a thin turbulent narrow current flowing under a still water and over a regular mild slope, in hydrostatic pressure fields (Smith 1973). None of these properties are fully satisfied in this strait. The internal Rossby radii are particularly small, and this could also give rise to current recirculation. On the other hand the topographic constraint seems to be strong enough to avoid this likelihood, and, in addition, reasonable results are obtained here by using such a model. So this remains an important open question, to be further discussed in a forthcoming numerical investigation.

Acknowledgments. We must thank the two reviewers for their helpful comments and suggestions, Prof. M. Crepon for encouragement and help, and ASI and SINAPSI for economic support. Finally, we must thank R. De Gregorio, L. Santonastaso, and R. Soldatelli for warm collaboration. Mireno Borghini, Carlo Galli, and Egisto Lazzoni, from IOF, played a major role in the collection, analysis, and archiving of the collected data. The authors are also grateful to the Saclantcen of La Spezia for the possibility of periodically testing the CTD sonde in their calibration bath. Measurements were supported by the following EC-MAST Projects: EUROMODEL I and II (MAST - CT 90-0043-C and MAS -CT93-0066), GEODYME (MAS2-CT93-0061), and MATER (MAS3-CT96-0051), and by the CNR Physical Committee.

APPENDIX A

The Case of the Strait of Sicily

We now explicitly apply to the Strait of Sicily the dynamic considerations related to (3)–(6), namely a multilayer hydraulic exchange in a rather narrow strait. Taking ξ as alongstrait coordinate from east toward west, we can write

$$\frac{\partial}{\partial\xi}\left(\frac{1}{2}V_1^2 + gh_1\right) = \frac{1}{\mathcal{A}_1}\mathcal{M}_1 \tag{A1}$$

relative to MAW flowing eastward. For the LIW flowing westward we have

$$\frac{\partial}{\partial\xi}\left(\frac{1}{2}V_2^2 + g\frac{\rho_2 - \rho_1}{\rho_2}h_2 + g\frac{\rho_1}{\rho_2}h_1\right) = \frac{1}{\mathcal{A}_2}\mathcal{M}_2, \tag{A2}$$

and for the EMDW, also flowing westward,

$$\frac{\partial}{\partial\xi}\left(\frac{1}{2}V_3^2 + g\frac{\rho_3 - \rho_2}{\rho_3}h_3 + g\frac{\rho_2 - \rho_1}{\rho_3}h_2 + g\frac{\rho_1}{\rho_3 h_1}\right) = \frac{1}{\mathcal{A}_3}\mathcal{M}_3. \tag{A3}$$

Consequently, from (A2) and (A3) we have

$$\frac{\partial}{\partial\xi}\left[\frac{1}{2}V_3^2 + g\frac{(\rho_3 - \rho_2)}{\rho_3}h_3\right] = \frac{1}{\mathcal{A}_2}\mathcal{M}_3 + \frac{\rho_2}{\rho_3}\left(\frac{\partial}{\partial\xi}\frac{1}{2}V_2^2 - \frac{\mathcal{M}_2}{\mathcal{A}_2}\right), \tag{A4}$$

where $\mathcal{M}_2$ only accounts for stresses between layers, while $\mathcal{M}_3$ includes also the bottom stress.

Following the same parameterization of Baringer and Price (1997a,b), we have

$$\mathcal{M}_2 = E'W(V_2 - V_1)^2 - E^*W(V_3 - V_2)^2$$
$$\mathcal{M}_3 = E^*W(V_3 - V_2)^2 - KWV_3^2, \tag{A5}$$

where E' and E^* are entrainment parameters, K is the drag coefficient, and W is the cross-sectional area. All stresses are integrated across each section.

It is interesting to note that the bottom stress and the effect of MAW–LIW interaction are opposite in sign, and this constitutes a fundamental effect, finally accelerating the deep EMDW current toward the sill.

Not all the stresses are of the same order of magnitude. The largest are the bottom stress KWV_3^2 and the entrainment between the first (MAW) and second (LIW) layers, because MAW and LIW flow in opposite directions. The entrainment between the second (LIW) and the third (EMDW) layers, due to the small difference between LIW and EMDW velocity, is generally weaker.

The previous considerations can be applied to Eq. (10) and (11), where now U indicates the EMDW along-vein velocity.

APPENDIX B

Perturbative Treatment of Uncompressibility and Steady Momentum Equations (14)

Let us rapidly outline a perturbative treatment of (14). Since E^* and K are relatively small quantities compared with the other terms in (14), these equations can be solved as

$$\mathcal{A}U = hWU = \mathcal{A}_0U_0 + \int_0^\xi E^*W|U - V_2|\,d\xi'$$
$$\sim \mathcal{A}_0U_0 + E^*W|U_0 - V_2|\xi + \cdots$$
$$\frac{\partial}{\partial\xi}\left\{U^2\mathcal{A} + g'\mathcal{A}\left[b + \frac{\mathcal{A}_0U_0 + E^*W|U_0 - V_2|\xi}{2WU}\right] + \cdots\right\}$$
$$+ KWU^2 - \mathcal{D} = 0. \tag{B1}$$

Note that we can write (B1) as

$$\frac{\partial}{\partial\xi}\left(U^2\mathcal{A} + g'\mathcal{A}\left[b^* + \frac{\mathcal{A}_0U_0}{2UW}\right]\right) = \mathcal{D}, \tag{B2}$$

introducing a kind of fictitious sea bottom,

$$b^* \rightarrow b + \frac{E^*|U_0 - V_2|}{2U_0}\xi + \frac{WKU_0^2}{g'\mathcal{A}}\xi. \qquad \text{(B3)}$$

In practice, we can either discuss (B3) as in Gill (1977) or the differential equation

$$\frac{\partial}{\partial\xi}\left(U^2\mathcal{A} + g'\mathcal{A}\left[b + \frac{\mathcal{A}_0U_0}{2UW} + E\frac{(U_0 - V_2)}{2U}\xi\right]\right) + KWU^2 - \mathcal{D} = 0, \qquad \text{(B4)}$$

namely an ordinary nonlinear differential equation that is readily solved numerically.

REFERENCES

Astraldi, M., G. P. Gasparini, M. Moretti, E. Sansone, and S. Sparnocchia, 1996: The characteristics of the water masses and the water transport in the Sicily Channel at long time scales. *Dynamics of Mediterranean Straits and Channels,* F. Briand, Ed., Bulletin de l'Institut Océanographique, Monaco, No special 17, CIESM Science Series 2.

Baringer, M., and J. Price, 1997a: Mixing and spreading of the Mediterranean outflow. *J. Phys. Oceanogr.,* **27,** 1654–1677.

——, and ——, 1997b: Momentum and energy balance of the Mediterranean outflow. *J. Phys. Oceanogr.,* **27,** 1678–1692.

Bignami, F., G. Mattietti, A. Rotundi, and E. Salusti, 1990: On a Sugimoto–Whitehead effect in the Mediterranean Sea: Fall and mixing of a bottom current in the Bari canyon, Southern Adriatic Sea. *Deep-Sea Res.,* **37,** 657–665.

Chapman, D., and G. Gawarkiewicz, 1995: Offshore transport of dense shelf water in the presence of a submarine canyon. *J. Geophys Res.,* **100,** 13 373–13 387.

Ellison, T., and J. Turner, 1959: Turbulent entrainment in stratified flows. *J. Fluid Mech.,* **6,** 423–448.

Emms, P., 1997: Streamtube models of gravity currents in the ocean. *Deep-Sea Res.,* **44,** 1575–1610.

Gill, A., 1977: The hydraulics of rotating channel flow. *J. Fluid Mech.,* **80,** 641–671.

Killworth, P., 1977: Mixing on the Weddell Sea continental slope. *Deep-Sea Res.,* **24,** 427–448.

Kinder, T., and H. Bryden, 1990: Aspiration of deep waters through straits. *The Physical Oceanography of Sea Straits,* L. Pratt, Ed., Kluwer Academic, 295–319.

Lane-Serff, G. F., D. A. Smeed, and C. R. Postlethwaite, 2000: Multilayer hydraulic exchange flows. *J. Fluid Mech.,* **416,** 269–296.

Pratt, L. J., H. E. Duse, S. P. Murray, and W. Johns, 2000: Continuous dynamical modes in straits having arbitrary cross sections, with applications to the Bab el Mandab. *J. Phys. Oceanogr.,* **30,** 2515–2534.

Salusti, E., and F. Travaglioni, 1985: Currents and countercurrents in straits. *Oceanol. Acta,* **8,** 197–206.

Smith, P., 1973: The dynamics of bottom boundary currents in the ocean. Ph.D Thesis, Rep. 73-4, Rep. GFD/73-5, MIT, 205 pp.

——, 1975: A streamtube model for bottom boundary currents in the ocean. *Deep-Sea Res.,* **22,** 853–873.

Sparnocchia, S., G. P. Gasparini, M. Astraldi, M. Borghini, and P. Pistek, 1999: Dynamics and mixing of the eastern Mediterranean outflow in the Tyrrhenian basin. *J. Mar. Syst.,* **20,** 301–317.

Turner, J., 1986: Turbulent entrainment: The development of the entrainment assumption, and its application to geophysical flows. *J. Fluid Mech.,* **173,** 431–471.

Whitham, G., 1955: The effect of hydraulic resistance in the dam-break problem. *Proc. Roy. Soc. London,* **227A,** 399–407.